Relation between switching and conduction mechanisms in ferroelectric HZO 3D Capacitors

Constantin Le Grand de Mercey[1,2,†], Terry François[1], Marios Barlas[1*], Damien Deleruyelle[2], Kristell Jouannic[1], Xavier Federspiel[1], Simon Jeannot[1], Olivier Noblanc[1]

[1]STMicroelectronics, 850 Rue Jean Monnet, 38920 Crolles, France

[2] INSA Lyon, Ecole Centrale de Lyon, CNRS, Universite Claude Bernard Lyon 1, CPE Lyon, INL, UMR5270, 69621 Villeurbanne, France

[†]E-mail : constantin.legranddemercey@st.com, *E-mail : marios.barlas@st.com

***Abstract*— This work provides a comparative study of solid-solution and superlattice FE-HZO of varying compositions deposited by ALD supercycling integrated in 3D MIM devices, in a 40 nm platform. Remanent polarization, programming endurance and wake-up are co-optimized for 8nm thin films allowing 1.2V operation with the superlattice stack, achieving higher 2·Pr while minimizing wake-up and improving cycling endurance compared to the solid-solution counterparts. The role of dielectric versus ferroelectric-switching related ageing is decorrelated by a combination of conduction mechanism analysis as well as unipolar and bipolar TDDB measurements, highlighting the differing roles of the read and programming operation in the MIM lifetime.**

Keywords- ferroelectrics, HZO, FeCAP, 3D capacitor, superlattice, endurance, reliability, FORC, conduction

I. INTRODUCTION

Ferroelectric capacitors (FeCAPs) are strong contenders to enable embedded non-volatile memories (eNVM) or DRAMs for edge AI and compute-in-memory (CiM) workloads [1]. To achieve optimal performance, ferroelectric (FE) memories must be carefully optimized both in the circuit level and, upstream, at the material level. While 3D architectures have already been demonstrated in advanced-node integrated circuits [2] and the benefits of introducing multilayers [3,4] depositions forming superlattice (SL) stacks have been reported, the underlying reliability physics of such devices has not yet been studied in detail. Here, we perform a systematic exploration of ferroelectric nanolaminate and solid-solution ferroelectric layers, integrated in 3D MIMs from the standpoint of ferroelectric performance, conduction mechanisms, and TDDB reliability to identify the interplay between material structure, and ferroelectric switching in device lifetime.

II. DEVICE DESCRIPTION

3D ferroelectric MIM capacitors were fabricated in the BEOL of a 40nm CMOS node (Fig. 1a). Ferroelectric $Hf_xZr_yO_2$ films were deposited by super-cycling ALD process, in which Zr to Hf precursor cycles are alternated at each cycle to form a solid solution (SS-HZO) or over x and y monolayers to create multilayer superlattices (SL-HZO) (Fig. 1b). In total 3 different stacks were designed: An equimolar Hf to Zr content SS-$Hf_{0.5}Zr_{0.5}O_2$, a Zr-rich SS-$Hf_{0.3}Zr_{0.7}O_2$ and a Zr-rich superlattice SL-$Hf_{0.3}Zr_{0.7}O_2$. In the following, the tested capacitors are integrated in arrays as shown in the TEM image (Fig.1c).

III. FE STACK PERFORMANCE AND RELIABILITY

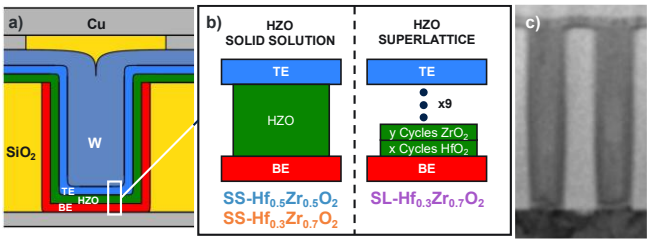

Figure 1 (a) Schematic of cross-section of 3D MIM capacitors (b) ALD deposited stack. solid solution (SS-HZO): cycle-to-cycle to cycle alternation versus Superlattice (SL) SL-HZO alternation every x and y cycles of HfO_2 and ZrO_2 precursors, respectively. (c) TEM Image within a device array.

In this section devices under test (DUTs) were cycled at 100kHz using square pulses (SQ) with different stress levels (3, 3.5, 3.75MV/cm). SQ pulses have 100ns rise and fall times and are applied without relaxation time, resulting in a 100% duty-cycle stress. Thin films polarization was extracted from PUND measurements, at ±4MV/cm and 100kHz [5]. Complete switching of the ferroelectric layers was verified by checking switching efficiency (defined in section V). Figure 2 presents the mean remanent polarization obtained on 16 FeCAP arrays (150 DUTs/array) for the three stacks at different stress fields.

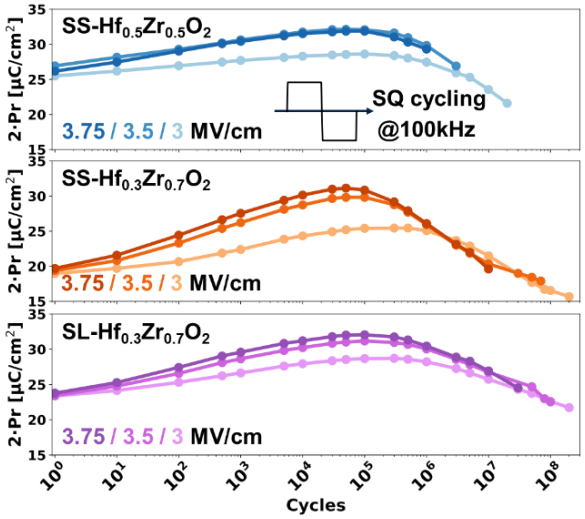

Figure 2 Remanent polarization cycling endurance for (a) SS-$Hf_{0.5}Zr_{0.5}O_2$ showing limited endurance (b) SS-$Hf_{0.3}Zr_{0.7}O_2$ and (c). SL-$Hf_{0.3}Zr_{0.7}O_2$ The Zr-rich SS sample (b) exhibit improved cycling endurance at the expense of stronger wake-up. The Zr-rich SL-HZO (c) optimizes the tradeoff between endurance enhancement and wake-up. Mean of 16FeCAPs arrays (150DUTs/array).

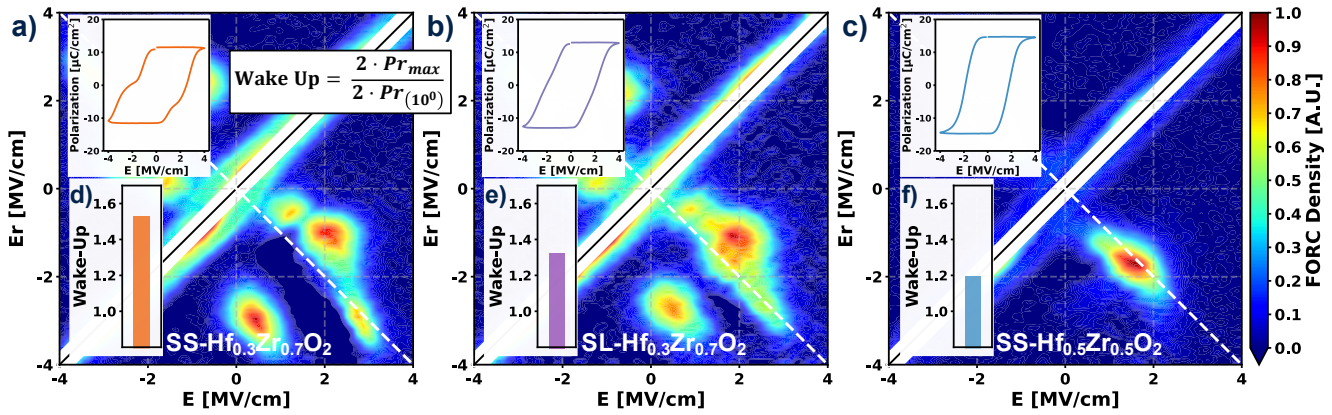

Figure 3 FORC density maps after 100 cycles for (a) SS-$Hf_{0.3}Zr_{0.7}O_2$ (b) SL-$Hf_{0.3}Zr_{0.7}O_2$ and (c) SS-$Hf_{0.5}Zr_{0.5}O_2$ showing the Zr doping related spread of domains distribution in pristine samples with their related polarization loop. (d), (e), and (f) are respectively the associated wake-up ratios of each device correlating with the broader distribution of domains.

The SS-$Hf_{0.5}Zr_{0.5}O_2$ samples exhibit the highest 2·Pr together with a low to no wake-up. SL-$Hf_{0.3}Zr_{0.7}O_2$ displays reduced wake-up and fatigue compared to SS-$Hf_{0.3}Zr_{0.7}O_2$ while maintaining a slightly higher 2·Pr at 10^5 cycles. Figure 3 shows first-order reversal curve (FORC) spectroscopy and the associated wake-up ratio of each film. The wake-up ratio is defined in the insets, where $2 \cdot Pr_{max}$ and $2 \cdot Pr_{(10^0)}$ are the maximum remanent polarization achieved and the remanent polarization in the pristine state, respectively. FORC was performed after 100 cycles with 40mV steps and 1MV/s sweep-rate. The broad domain distributions in Fig. 3a and 3b are attributed to the Zr concentration, which promotes tetragonal phase crystallization and anti-ferroelectric behavior [6]. The domain distributions progressively merge during cycling leading to 2Pr increases and wake-up. A clear correlation between the domain spread (Fig. 3 a-c) and the wake-up ratio (Fig. 3 d-f) is noted for all the three stacks. The multilayer deposition (Fig. 3b) yields a more homogenous domain distribution compared to the SS-$Hf_{0.3}Zr_{0.7}O_2$ sample (Fig. 3a).

The Cycle to breakdown (CTB) values for each FeCAP array were grouped to build Weibull distributions, from which the T_{63} values were extracted (Fig. 4) for each stress conditions.

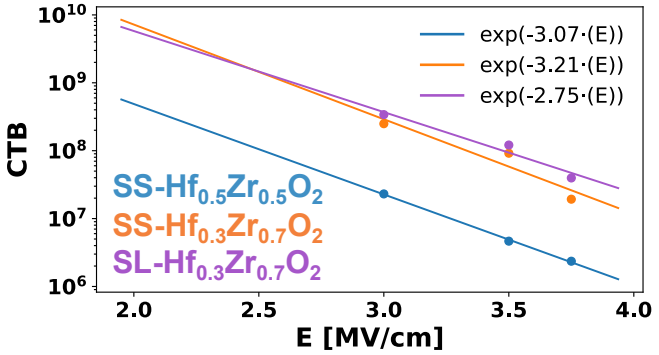

Figure 4 CTB versus cycling stress fields. Zr-rich materials have a better endurance over the SS-$Hf_{0.5}Zr_{0.5}O_2$.

The data allows to estimate the CTB trends by extrapolation, indicating better endurance for the two Zr-rich stacks over the SS-$Hf_{0.5}Zr_{0.5}O_2$. However, device true lifetimes may yet be significantly different at lower fields and high-cycle testing is time-consuming. To go further is required firstly to understand the role of dielectric conduction versus that of ferroelectric switching in defect generation over time. This requires studying both conduction and TDDB mechanisms.

IV. CONDUCTIVITY IN 3D FE CAPACITORS

The dielectric conduction mechanisms were investigated by temperature-dependent I-V measurements under negative bias (Fig5 a-c, median *logJ-logE* of 16 FeCAParrays of 150k DUTs shown). To subtract transient dielectric relaxation effects a wait time of 12s at each point was introduced [7]. All stacks exhibit similar low- and high-field conduction regimes, while SS-$Hf_{0.5}Zr_{0.5}O_2$ shows an additional intermediate-field regime (Fig. 5a). In Fig. 5d-f, the films conductivity (σ) is plotted versus temperature and follows well a 3D Mott-like variable range hopping regime (VRH) [8], as seen from the $T^{-1/4}$ dependence., following assessment of various conduction mechanisms. At low fields, the dependence of conductivity to temperature weakens (decreasing slope of $log(\sigma)$-$T^{-1/4}$). This can be explained by introducing field-dependence in the slope (Fig. 5g) using the Apsley-Hues model [9,10], where E is the electric field, T the temperature, σ_0, T_0 and E_0 are fitting parameters of the resulting relation. The data is in good agreement with the linearized $log(\sigma)$-$T^{-1/4}$ law implying a proportional relationship between E_0 and T. Thus, the Mott characteristic temperature T_0 can be extracted (Fig. 5h), where k is the Boltzmann's constant, $N(E_F)$ is the density of states at the Fermi level, and a the localization length. Assuming a as a common parameter across the three materials (attributed to the formation of an oxygen vacancy), the relative variation of $N(E_F)$ between samples is reported (Fig. 5i) with SS-$Hf_{0.5}Zr_{0.5}O_2$ as the reference stack. A higher relative $N(E_F)$ value points to a more trap rich material in the pristine state. Contrary to the low-field region, the slope of σ increases with E. This is consistent with trap-assisted tunnelling conduction, yet more detailed investigation might be required to fully quantify this regime. Breakdown electric fields (E_{bd}) under negative bias were measured at three temperatures (-40°C, 25°C, 125°C) (Fig. 6). The three stacks exhibit similar E_{bd} and β (Weibull slope) values for given temperature conditions.

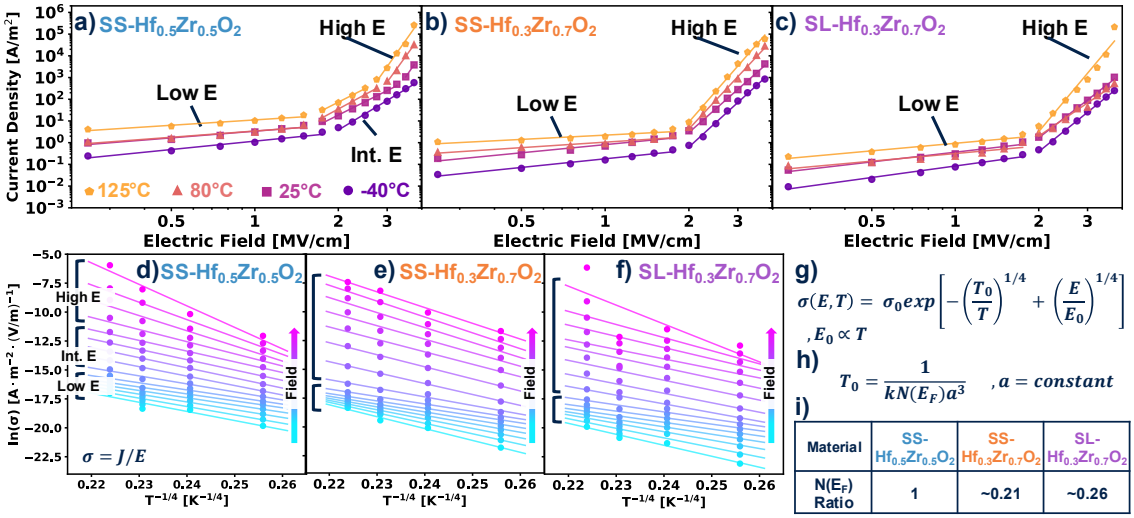

Figure 5 (a-c) I-V curves under negative bias showing distinct low, intermediate, and high field regimes. Mean of 16 FeCAP arrays (150k DUTs/array) per condition. (d-f) Conductivity versus temperature fitted with 3D Mott's VRH. (g, h) Field dependent VRH model and extraction of T_0 and $N(E_F)$. (i) Comparison of $N(E_F)$, highlighting higher defect states in SS-$Hf_{0.5}Zr_{0.5}O_2$.

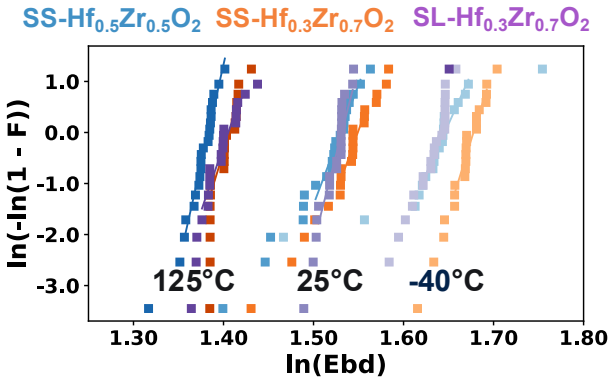

Figure 6 E_{bd} of FE films at (-40°c, 25°c and 125°c) under negative bias. Populations of 20 FeCAP arrays (1500DUTs/array)

Modest temperature dependence is observed, consistent with the high field dominated behavior and temperature dependence identified in this range (Fig. 5). The similar values of β point to an equivalent critical defect density for all stacks [11]. Hence defect generation owed to dielectric leakage is expected to be comparable across all stacks as, in the high-field region the conduction regime is comparable across all samples in terms of both field/temperature dependence and current density values. Therefore, the endurance gap observed between stacks (Fig. 4) cannot be explained by dielectric leakage alone, especially at fields comparable to the magnitude of the programming pulse. The difference in E_{bd} values (Fig.7a) under positive and negative stress points towards some level of interface asymmetry between top and bottom electrodes (BE, TE), further supported by asymmetry in the conduction (Fig.7b). This imposes the need to examine the behavior of TDDB in both positive and negative bias. Furthermore, it implies that the BE interface density is higher as compared to the TE, originating from the integration scheme of the 3D-FeCAP.

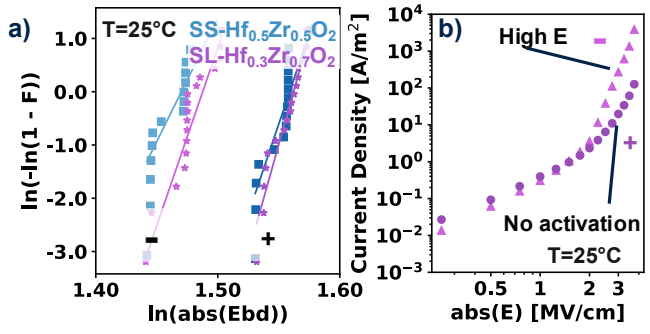

Figure 7 (a) E_{bd} of FE stacks under positive and negative bias. Populations of 16 FeCAP arrays (1500DUTs/array). (b) SL-$Hf_{0.3}Zr_{0.7}O_2$ I-V curves with positive and negative bias. Mean of 16 FeCAP arrays (1.5M DUTs/array).

V. TDDB UNDER DC AND AC STRESS

DC TDDB measurements were performed at 25°C for the 8nm SL-$Hf_{0.3}Zr_{0.7}O_2$ stack. The cumulative time to breakdown (TDDB) distributions are shown in Fig. 8 with a sampling of 16 arrays (1.5M DUTs/array) per condition. TDDB lifetime is higher in positive bias (DC+) than in negative bias (DC-) indicating a defect rich BE, by comparison. The corresponding T_{63} values of the Weibull distributions follow a square root dependence on the electric field (Fig. 9). The difference between positive and negative constant voltage stress appears as a leftward shift of negative biased TDDB. Both positive and

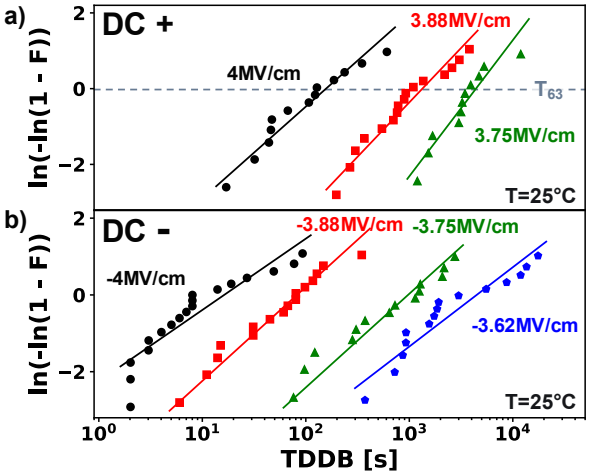

Figure 8 Time to breakdown distributions under increasing E-field at 25°C for the SL- SL-$Hf_{0.3}Zr_{0.7}O_2$ sample with (a) positive and (b) negative bias. 16 arrays (1.5M DUTs/array) were measured field per condition.

negative bias DC TDDB exhibit similar field dependence. DC+ and DC- TDDB extrapolations converge towards lower fields, where the common low field conduction regime is dominant (Fig. 7b). To assess the impact of polarization reversal on thin-film reliability, CTB of Fig. 4 were mapped to the equivalent cumulative stress time ($t_{total} = N_{cycle} \cdot T_{pulse}^{FWHM}$) . Under bipolar AC switching stress, the SL-$Hf_{0.3}Zr_{0.7}O_2$ stack exhibits significantly lower TDDB lifetime compared to the DC cases. The nearly flat *TDDB-sqrt(E)* slope indicates that the defect generation owed to FE switching is dominant versus that owed to dielectric leakage. If all domains switch as is the case when using high-field pulses (≥ 3MV/cm) FE domains get reorganized, leading to accelerated ageing.

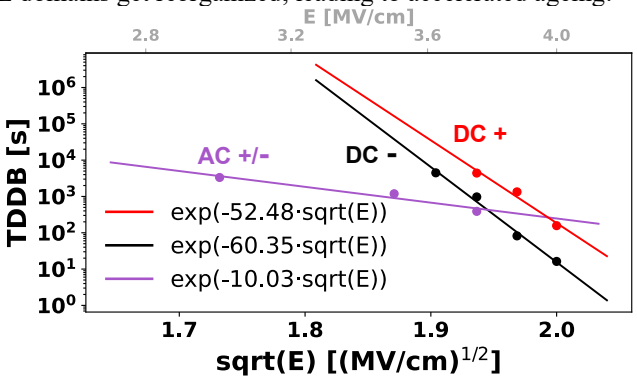

Figure 9 TDDB of SL-$Hf_{0.3}Zr_{0.7}O_2$ under DC and AC stress. Under AC condition device has a lower slope and TDDB, revealing the negative impact of domain reversal on thin film endurance.

To quantify the impact of partial domain switching in device lifetime, the switching efficiency (S_{Eff}) is calculated (fraction of switched domains during programming). S_{Eff} is defined as the ratio of the switching current from a programming pulse at a given stress field (E_{Stress}) to the switching current of the 4MV/cm PUND pulse taken as reference (Fig. 10a). The resulting effective 2·Pr ($2 \cdot Pr_{Eff}$) allows to discriminate full, from partial domain switching (Fig. 10b). For low E-field, the SS-$Hf_{0.5}Zr_{0.5}O_2$ stack maintains higher 2·Pr values as compared to the two other films even at 1.5MV/cm owed to its "unimodal" domain distribution. The discrete, 'multimodal" distributions of the Zr-rich samples allow to switch different domain regions individually. This leads to not only a clearer separation of programmed states (Fig 10b), but also to total endurance enhancement. The superlattice structure allows to optimize that behavior: At 1.5MV/cm, both wake-up and fatigue are significantly reduced after 10^9 cycles (test time limited). Three discrete memory states can be stably programmed in the SL- $Hf_{0.3}Zr_{0.7}O_2$ stack. Fig. 10c shows the endurance and the $2 \cdot Pr_{Eff}$ (from Fig. 10b) versus S_{Eff} at 10^5 cycles, clearly illustrating the correlation between lower S_{Eff} and higher endurance. Moreover, it highlights the difference in the resulting S_{eff} between stacks at a given cycling condition.

VI. CONCLUSIONS

This work explores the method of film deposition and its composition to the wake-up and fatigue behavior. By systematic conduction mechanism analysis and TDDB measurements we demonstrate the dominant role of FE domain switching in the ageing of 3D-FeCAPs. By partially switching discrete FE domains, the overall device endurance can be extended. It points towards the potential of non-destructive readout schemes to significantly improve FeRAM device

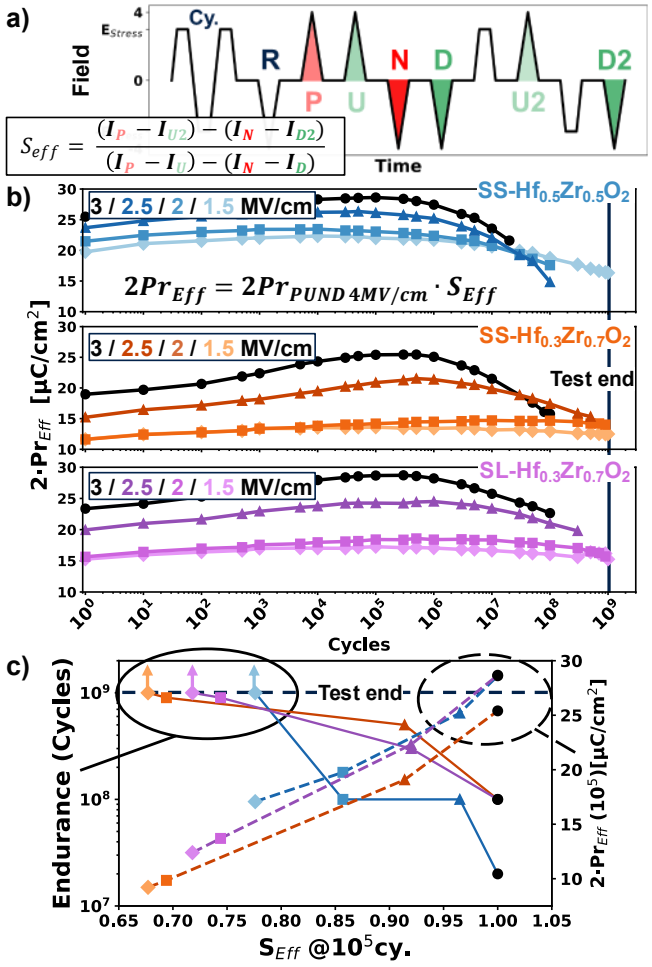

Figure 10 (a) PUND and S_{Eff} measurement protocol. From each stress condition results a different S_{Eff} (b) Effective 2·Pr endurance for all stacks. (c) Endurance and effective 2·Pr at 10^5 cycles as a function of S_{Eff} at 10^5 cycles, showing the correlation between lower switching efficiency and higher endurance.

lifetimes. Superlattice deposited Zr rich HZO reduces both wake-up and fatigue effects in BEOL integrated 3D-FeCAPs while allowing to create discrete FE regions that can be stably programmed over cycling. Devices show improved endurance and stable polarization at 1.2V programming pulses (8nm films), demonstrating full compatibility with advanced CMOS nodes. Superlattice ALD can be an effective path for the engineering of multiple, discrete, remanent polarization domains that can be individually programmed across many cycles. The combined material and device operation approach can potentially pave the way for multi-bit high endurance FeRAM.

VII. REFERENCES

[1] S. Deng *et al.*, *IEDM*, pp. 1-4, **2024**. [2] Y. Sun *et al.*, *VLSI Technology and Circuits*, pp. 1-3, **2025**. [3] M. Habibi *et al.*, *Adv. Electron. Mater.*, 11, 2400764, **2025**. [4] Zhibin Yang *et al.*, *Journal of Alloys and Compounds*, 1004, **2024**. [5] I. Fina, *et al., Journal of Applied Physics*, vol. 109, p.074105, **2011** [6] Jianguo Li *et al.*, *Jpn. J. Appl. Phys.*, 63 12SP13, **2024**. [7] A.G. Viey, *et al.*, *IEDM*, pp. 1-4, **2025** [8] N. F. Mott, *Phil. Mag.*, 19, 35, **1969**. [9] N. Apsley & H. P. Hughes, *Phil.Mag.,* 30:5, 963-972, **1974**. [10] N. Apsley & H. P. Hughes, *Phil.Mag.,* 31:6, 1327-1339, **1974**. [11] J. Sune *et al.*, *IEEE El3ctron Device Letters*, 22, 6, pp. 296-298, **2001**.